THE JOURNAL OF PHYSICAL CHEMISTRY B

Article

pubs.acs.org/JPCB

Effect of Ion Rigidity on Physical Properties of Ionic Liquids Studied by Molecular Dynamics Simulation

Pedro E. Ramírez-González,[†] Gan Ren,[†] Giacomo Saielli,[‡] and Yanting Wang*,[†]

[†]CAS Key Laboratory of Theoretical Physics, Institute of Theoretical Physics, Chinese Academy of Sciences, 55 East Zhongguancun Road, P.O. Box 2735, Beijing 100190, China

[‡]Istituto per la Tecnologia delle Membrane del CNR, Sezione di Padova, Via Marzolo, 1, 35131 Padova, Italy

ABSTRACT: In this work, we have performed molecular dynamics (MD) simulations to compare the structural and dynamical properties of three ionic liquids (ILs), 1-ethyl-3-methyl-imidazolium tetrafluorborate ($[EMI^+][BF_4^-]$), 1,1′-dimethyl-4,4′-bipyridinium bis(tetrafluorborate) ($[VIO^{2+}][BF_4^-]_2$), and 1,1′-dimethyl-4,4′-bipyridinium bis(trifluoromethylsulfonyl)imide (bistriflimide in short) ($[VIO^{2+}][Tf_2N^-]_2$), aiming to discover the influence of ion rigidity on the physical properties of ILs. $[VIO^{2+}]$ is more rigid than $[EMI^+]$, and $[BF_4^-]$ is more rigid than $[Tf_2N^-]$. $[VIO^{2+}][BF_4^-]_2$ has an anion distribution different from the other two by the higher and sharper peaks in the cation−anion radial distribution functions, reflecting a close-packed local structure of anions around cations. $[VIO^{2+}][BF_4^-]_2$ and $[VIO^{2+}][Tf_2N^-]_2$ have similar dynamics much slower than $[EMI^+][BF_4^-]$, and $[VIO^{2+}][Tf_2N^-]_2$ shows a more isotropic molecular distribution than $[VIO^{2+}][BF_4^-]_2$ and $[EMI^+][BF_4^-]$. Additionally, we have simulated two modified viologen-based ILs to reinforce our interpretations. We conclude from the above simulation results that the rigidity of anions influences the alignment of cations and that the rigidity of cations shows a large obstacle to their rotational capacity. Moreover, we have observed a slower diffusion of $[VIO^{2+}][BF_4^-]_2$ due to the electrostatic correlations, which stabilizes the ion-cage effect.

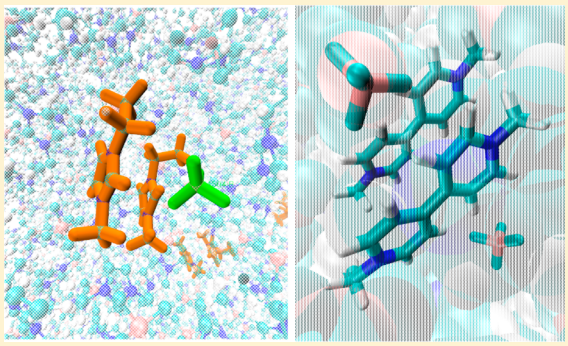

1. INTRODUCTION

Coulombic fluids are liquids formed solely or mostly by charged components.[1] The classic examples of this kind of fluids are molten salts, electrolytic solutions, and liquid metals.[2] In recent years, a large number of organic salts with near-room-temperature melting points have been developed.[3−5] The study of those novel compounds, usually called room-temperature molten salts or simply ionic liquids (ILs), has become a very active field due to their promising applications in industry.[6,7]

The pyridinium-based[8] and imidazolium-based[9] ILs were synthesized around 1980s. Since then, a lot of experimental, theoretical, and simulation works have been done to understand their physical and chemical properties. However, due to the great diversity of ILs, a lot of open questions still remain unanswered. For instance, the key effects that govern the phase behavior of ILs are not fully understood.

The 1,1′-dialkyl-4,4′-bipyridinium salts, usually known as viologens, attract a lot of research interest because of their interesting redox behavior.[10,11] They can form viologen-based ILs when combined with appropriate anions, which exhibit liquid crystal (LC) mesophases with long cationic side chains and flexible anions.[12−15] These mesophases, known as ionic liquid crystals (ILCs), are a special group of chemicals combining the properties of both ILs and LCs. Besides several ILs that have been found to exhibit a strong tendency of ordering into a Smetic-A (SmA) structure,[16−18] Bhowmik and co-workers[19,20] have made an interesting series of experiments on symmetric viologen cations combined with inorganic and organic anions and concluded that the use of the bis(trifluoromethylsulfonyl)imide (bistriflimide or Tf_2N^-) anion permits the appearance of stable ILC mesophases. Additional experiments demonstrated that the ILC phases can be stabilized in a wide range of temperatures when a moderate asymmetry of the alkyl side chains is introduced.[21] However, it has been proved that the methylation of the pyridinium core suppresses the ILC mesophase.[22] Recently, the flexibility of alkyl chains or anions was found to play a key role in forming the ILC structure for viologen dimers.[23,24] All of the experimental studies done for viologen systems suggest a prominent role of the intrinsic rigidity of viologens in the phase behavior. Therefore, systematic theoretical studies of the structural and dynamical properties of these liquids are necessary for a deep understanding of their phase behavior and microscopic properties.

Despite the above studies on viologen-based ILs, their basic physical properties are still poorly understood. However, the imidazolium-based ILs have been the subject of extensive studies in recent years, and a much better understanding of

Received: April 3, 2016
Revised: June 3, 2016
Published: June 7, 2016

DOI: 10.1021/acs.jpcb.6b03379
J. Phys. Chem. B 2016, 120, 5678−5690

their properties have already been established. Some experiments have shown the importance of the cationic alkyl side-chain length on their physical properties, such as diffusion coefficient and mass density,[25−27] dielectric constant,[28] conductivity,[29] and ILC mesophases.[30−33] Molecular dynamics (MD) simulations revealed the influence of the cationic side-chain length on diffusion[34] and structure,[35] the long-range ordering of ions,[36] and the spatial[37] and dynamic[38] heterogeneities. Habasaki and Ngai[39] showed that imidazolium-based ILs have a strong tendency to behave as supercooled liquids. Recently, a systematic study revealed that the intrinsic electric field in ILs is only a little stronger than that in molecular liquids and much weaker than that in inorganic molten salts.[40] Monocationic and dicationic ILs[41] were compared in MD simulations, and significant structural differences were found for long alkyl chains. All of the above suggest that abundant studies on imidazolium-based ILs allow them a good choice of counterparts for investigating viologen-based ILs.

The rigidity of molecules seems to play an important role in forming ILC structures for both viologen-based and imidazolium-based ILs. Since the imidazolium cation is relatively flexible, the system is easier to be disordered and form the liquid phase. When it is combined with a rigid anion (Cl^-, BF_4^-, PF_6^-, etc.), the ILC structure appears at appropriate temperatures when the cationic side chain is sufficiently long.[30−33] In contrast, the liquid phase is more favorable when it is combined with a flexible anion such as Tf_2N^-. However, the more rigid viologen cation cannot form ILC phases when it is combined with a rigid anion, and the ILC phases can be observed only when it is combined with a flexible anion.

To obtain the preknowledge for understanding the microscopic mechanism of the ILC phase formation of viologen-based ILs and the influence of the molecular flexibility, we present a detailed comparison between an imidazolium-based IL, 1-ethyl-3-methyl-imidazolium tetraflourborate ($[EMI^+][BF_4^-]$), and a viologen-based IL, 1,1′-dimethyl-4,4′-bipyridinium bis(tetraflourborate), also called dimethyl-viologen tetrafluorborate, ($[VIO^{2+}][BF_4^-]_2$). The choice of the particular anion tetrafluorborate was intended to have a very rigid anion so that the cation flexibility can be clearly studied. Our simulation results indicate that $[VIO^{2+}][BF_4^-]_2$ has a much slower dynamics than $[EMI^+][BF_4^-]$ and that the former has a different anion distribution around cation from the latter, which can be attributed to the rigidity and the dicationic nature of the viologen-based IL. In order to distinguish the effects of the dicationicity and rigidity on molecular properties, further simulations of two modified viologen-based ILs were performed. In the first case, we have removed the constraint which keeps the two rings in the VIO^{2+} cation in the same plane, obtaining a flexible dication. The second case was an IL with the cationic total charge reduced to +1. Those simulations have shown a prominent role of the total charge of the cation on structural and dynamical properties. The rigidity of cations impacts principally on the mobility of the system and has only a marginal effect on the pair correlation functions.

We have also explored the effect of the anionic rigidity by performing an additional MD simulation of the 1,1′-dimethyl-4,4′-bipyridinium bistriflimide IL, also called dimethyl viologen bistriflimide ($[VIO^{2+}][Tf_2N^-]_2$). Our results show that the structural properties of $[VIO^{2+}][Tf_2N^-]_2$ are completely different from those with a rigid BF_4^- anion. Moreover, the dynamic properties of $[VIO^{2+}][Tf_2N^-]_2$ are almost the same as those of $[VIO^{2+}][BF_4^-]_2$.

2. SIMULATION AND ANALYSIS METHODS

2.1. Molecular Model. A schematic representation of the cations and the anions simulated in this work is drawn in Figure 1, where the two-ring structure is the viologen (VIO^{2+}) cation,

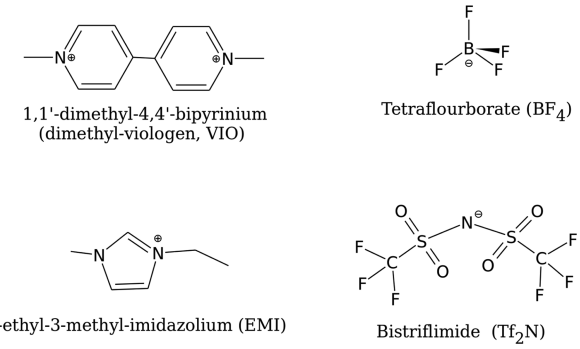

Figure 1. Molecular structures of the ions constituting the ILs studied in this work.

and the one-ring structure is the imidazolium (EMI^+) cation. The tetraflourborate (BF_4^-) anion has a tetrahedron structure, while the cations are essentially planar molecules. The bistriflimide (Tf_2N^-) anion is very flexible adopting many possible configurations.

The force field of EMI^+ was taken from ref 42, which is based on the AMBER force field.[43] The force field of BF_4^- was developed by J. de Andrade and co-workers.[44] The AMBER force field[43] was used to model the bonded and nonbonded interactions of the VIO^{2+} cation. The standard one-configuration two-step fitting procedure RESP[45] was used to determine the partial charges consistent with the AMBER force field as follows. The first step was using the Gaussian package[46] to obtain the ab initio optimized structure of the cation at the B3LYP/6-31g* level. The next step was obtaining the partial charges which best fit the electrostatic potential at the points selected according to the Merz−Singh−Kollman scheme at the HF/6-31g* level. The last step was calculating the partial charges compatible with the AMBER force field by the RESP package included in the AMBER tools software.[47] The obtained partial charges for VIO^{2+} are summarized in Table 1. The bonded and nonbonded parameters of the $[Tf_2N^-]$ anion were taken from Liu and Maginn's work,[48] but its partial charges were calculated with the RESP procedure (Table 1) to be consistent with the partial charges of bipirydinium. Despite the fact that the force field parameters have been taken from different sources, they are all compatible with the standard AMBER potential, so they should be consistent with each other.

2.2. Simulation Methods. All our simulations were performed with the GROMACS[49] MD simulation package. The periodic boundary condition (PBC) was applied to all three dimensions of a cubic simulation box, and a 1.6 nm cutoff was applied to the nonbonded interactions. The long-range electrostatic interactions were handled with the particle mesh Ewald (PME) method.[50] The $[EMI^+][BF_4^-]$ system contains 1024 ion pairs, $[VIO^{2+}][BF_4^-]_2$ contains 512 cations and 1024 anions, and $[VIO^{2+}][Tf_2N^-]_2$ contains 256 cations and 512 anions. To distinguish the effect of total charge and rigidity on

DOI: 10.1021/acs.jpcb.6b03379
J. Phys. Chem. B 2016, 120, 5678−5690

Table 1. Partial Charges for the Bipirydinium Cation and the Bistriflimide Anion Calculated with the RESP Method

atom	description	partial charge
CA1	ring member bonded to N	−0.013475
CA2	ring member not bonded to N	−0.128711
CA3	ring member bonded to the other ring	0.105547
N	in bipirydinium	0.111043
H4	bonded to CA1	0.221247
HA	bonded to CA2	0.181887
CT	methyl carbon	−0.183761
H1	methyl hydrogen	0.148425
N	in bistriflimide	−0.584243
S	in bistriflimide	0.782511
O	in bistriflimide	−0.448549
C	in bistriflimide	0.158312
F	in bistriflimide	−0.083868

viologen-based ILs, the first modified IL system with 512 cations and 1024 anions has a flexible dication by artificially switching off the improper torsion potential keeping the two rings in the same plane. The second one contains 1024 anions and the same number of [VIO$^+$] cations whose partial charges were artificially reduced by half.

In our study, we chose T = 500 K as one of the target simulation temperatures since the experiment has demonstrated[51] that this temperature is well above the melting temperature of [EMI$^+$][BF$_4^-$]. However, we cannot find in the literature the melting point of [VIO^{2+}][BF$_4^-$]$_2$. The experiments[20] have reported 638 K as the melting point of dimethylviologen bis(iodide) and 405 K for viologen bistriflimide. According to the empirical rule[1] for the melting temperature T_m of ILs $T_m(I^-) > T_m(PF_6^-) > T_m(BF_4^-) > T_m(Tf_2N^-)$, T_m of [VIO^{2+}][BF$_4^-$]$_2$ should fall in the range between 405 and 638 K. Therefore, we chose the other target simulation temperature to be T = 700 K, well above the melting point of [VIO^{2+}][BF$_4^-$]$_2$. The target temperature for [VIO^{2+}][Tf$_2$N$^-$]$_2$ is also T = 700 K in order to compare with [VIO^{2+}][BF$_4^-$]$_2$.

The simulated systems were equilibrated by a simulated annealing procedure as follows. The initial random configuration went through a series of *NPT* simulations at a constant pressure P = 100 atm and different temperatures from T = 2000 K down to 1500, 1000, 800, 600, and 500 K. At each temperature, the system was simulated for 1 ns. The last configuration was then equilibrated with a 1 ns *NPT* simulation at P = 1 atm and T = 500 K to obtain the average simulation volume V. After that, the system further went through another simulated annealing procedure in the *NVT* ensemble with the same temperature sequence and the determined V. The equilibrated configuration finally went through the production runs in the *NVT* ensemble at T = 500 and 700 K, respectively. The simulation durations for [EMI$^+$][BF$_4^-$] at both temperatures and [VIO^{2+}][BF$_4^-$]$_2$ at 700 K are 10 ns, and 20 ns for [VIO^{2+}][BF$_4^-$]$_2$ at 500 K to obtain reliable results for dynamical properties.

2.3. Structural and Dynamic Analysis. Besides the radial distribution function (RDF) and the spatial distribution function (SDF), the orientational order parameter $P_2[\theta(r)]$ between cations, defined as

$$P_2[\theta(r)] = \frac{1}{2}\langle 3\cos^2[\theta(r)] - 1\rangle = \frac{1}{2}\langle 3[\mathbf{r}_{ref}\cdot\mathbf{n}]^2 - 1\rangle \quad (1)$$

was also calculated to quantify the structural properties. As illustrated in Figure 2, θ is the angle between the normalized

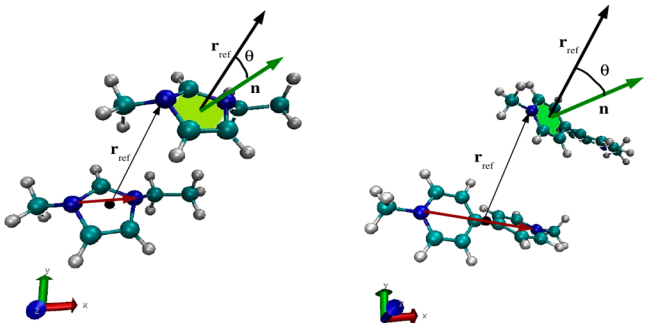

Figure 2. Illustration of the vectors involved in the definition of the orientational order parameters for EMI$^+$ (left) and VIO^{2+} (right).

reference vector $\mathbf{r}_{ref}$ and the vector $\mathbf{n}$. The vector $\mathbf{r}_{ref}$ points from the center-of-mass (COM) of a reference cation toward the nitrogen atom bonded to the methyl group of an adjacent cation. The unitary vector $\mathbf{n}$ is normal to the ring plane of the adjacent cation, and r is the magnitude of the reference vector $\mathbf{r}_{ref}$. The orientational order parameter takes a value close to zero if $\mathbf{n}$ are randomly distributed, and a finite value if $\mathbf{n}$ collectively have a preferred direction. In our calculations, only the ordering between cations was calculated because the anions do not have any particular planes for defining the alignment direction. Our orientational ordering parameter is close to the rotational ordering parameter defined in ref 52.

The dynamical properties were quantified with the mean-square displacement (MSD), the rotational autocorrelation function (RACF), and the ion cage correlation function (ICCF). The RACF quantifying the molecular rotational dynamics is defined as

$$P_2[\theta(r)] = \frac{1}{2}\langle 3\cos^2[\theta(t)] - 1\rangle = \frac{1}{2}\langle 3[\mathbf{R}(0)\cdot\mathbf{R}(t)]^2 - 1\rangle \quad (2)$$

where θ is the angle between the normalized vector $\mathbf{R}(0)$ pointing from one of the nitrogens to another one in the same cation at time t = 0 (the red vector in Figure 2) and the same vector $\mathbf{R}(t)$ at a later time t. The ICCF is defined as

$$S(t) = \frac{\langle p(0)p(t)\rangle}{\langle p(0)\rangle} \quad (3)$$

where $p(0)$ is unity if two counterions form a pair (distance less than 1.2 nm) at time 0 and zero otherwise, $p(t)$ is unity if two counterions form a pair at time 0 and remain a pair continuously until time t and zero otherwise, and <···> denotes the ensemble average over all ion pairs.

3. RESULTS: STRUCTURAL PROPERTIES

3.1. Radial Distribution Functions. It can be seen from Figure 3a that the maxima of $g_{++}(r)$ and $g_{--}(r)$ for [EMI$^+$][BF$_4^-$] coincide almost exactly with the minima of $g_{+-}(r)$ and the RDF oscillations extend until r = 2 nm, indicating a high degree of molecular structural ordering. In contrast, as shown in Figure 3b, for [VIO^{2+}][BF$_4^-$]$_2$, the $g_{++}(r)$ and $g_{--}(r)$ maxima do not coincide with the $g_{+-}(r)$ minima, and the $g_{--}(r)$ first peak is closer to the maximum of $g_{+-}(r)$. In addition, the cation−cation RDF has the first peak at a larger distance than the cation−anion RDF, and the RDFs oscillate

DOI: 10.1021/acs.jpcb.6b03379
J. Phys. Chem. B 2016, 120, 5678−5690

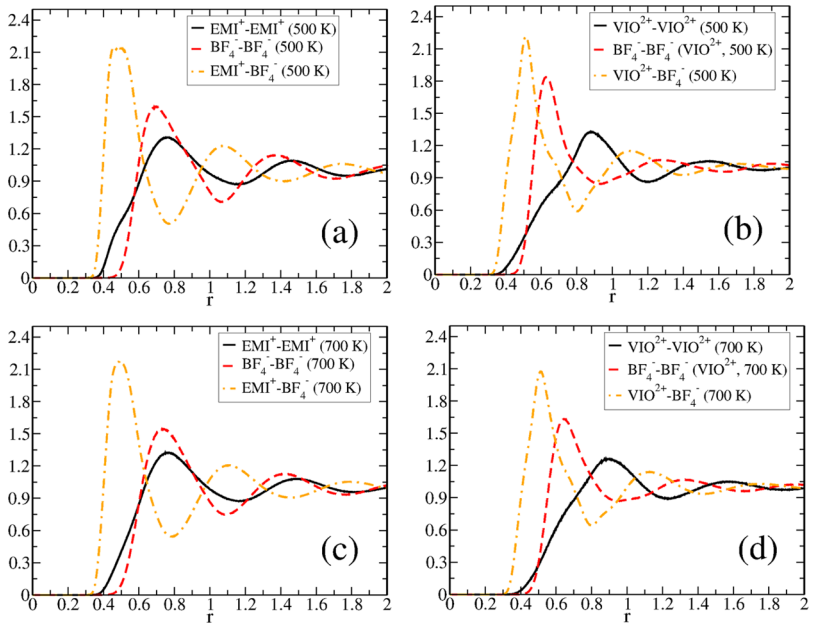

Figure 3. Radial distribution functions for the $[EMI^+][BF_4^-]$ and $[VIO^+][BF_4^-]_2$ ILs at P = 1 atm and T = 500 K (first row) or 700 K (second row). The g_{++}, g_{--}, and g_{+-} are plotted by solid, dashed, and dot-dashed lines, respectively.

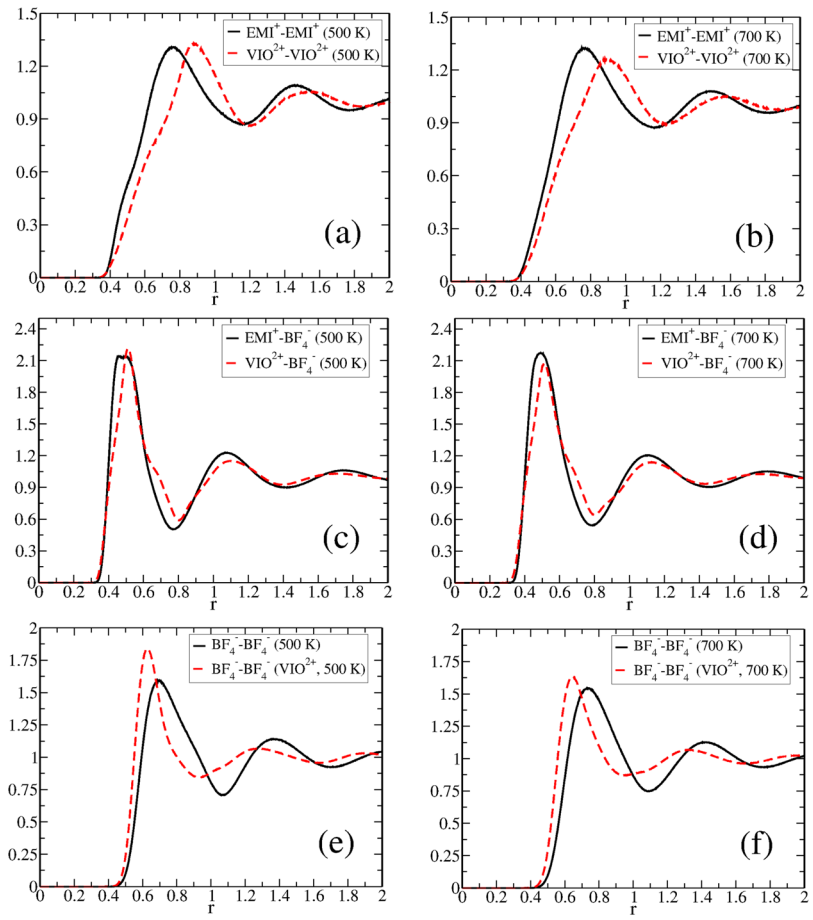

Figure 4. Comparisons between the cation−cation, cation−anion, and anion−anion RDFs in the first, second, and third rows, respectively. For all of the panels, the $[EMI^+][BF_4^-]$ RDFs are drawn in solid lines, and the $[VIO^{2+}][BF_4^-]_2$ RDFs are in dashed lines. Panels a, c, and e show the results at T = 500 K and b, d, and f for 700 K.

beyond r = 1.75 nm. The COM RDFs at T = 700 K, as shown in Figure 3, are similar to the ones calculated for T = 500 K.

The high degree of ordering exhibited in $[EMI^+][BF_4^-]$ RDFs due to the requirement of local neutrality is similar to the

DOI: 10.1021/acs.jpcb.6b03379
J. Phys. Chem. B 2016, 120, 5678−5690

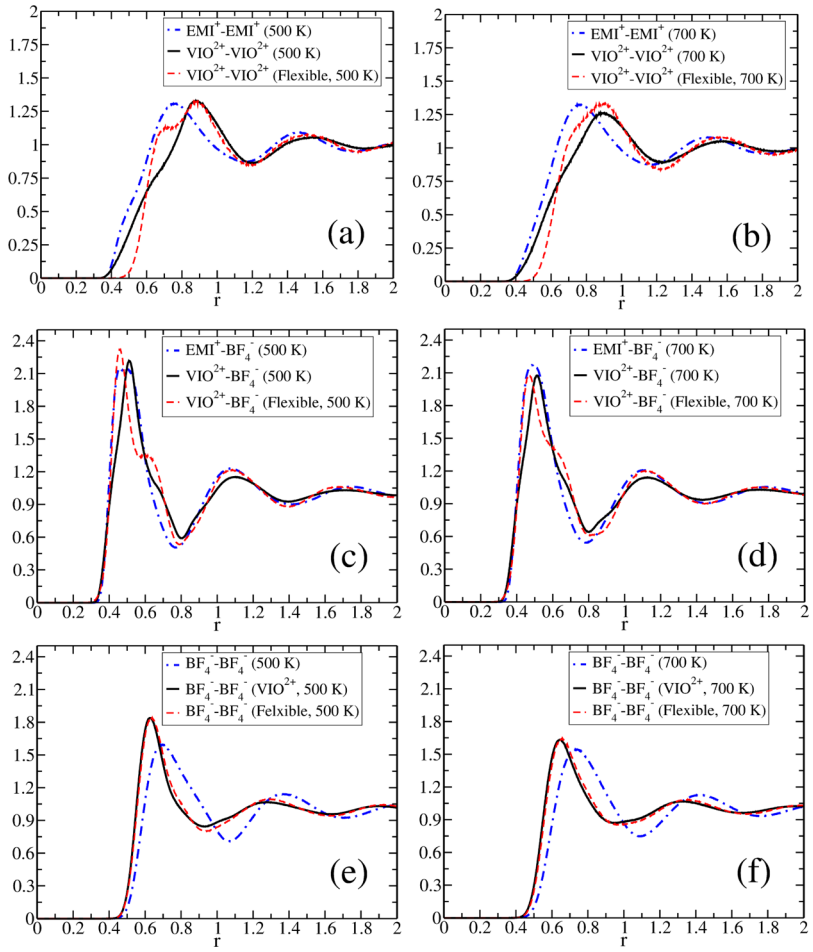

Figure 5. Comparison of the RDFs for the modified $[VIO^{2+}]$ $[BF_4^-]_2$ system with a flexible cation and the original system as well as the $[EMIM^+][BF_4^-]$ system. The left column shows the results at T = 500 K, and the right column is at T = 700 K. The top, middle, and bottom rows present the cation−cation, cation−anion, and anion−anion RDFs, respectively.

ordering observed in halide molten salts such as sodium chloride.[53] However, the observed shift of its peaks is attributed to the microscopic ordering of the counterions[37] due to the nonspherical charge distribution of $[EMI^+]$ and the size difference between cations and anions. However, the cation−cation and anion−anion RDFs of $[VIO^{2+}][BF_4^-]_2$ do not perfectly antiphase with the cation−anion RDF because the two positive charges of $[VIO^{2+}]$ require more surrounding anions than $[EMI^+]$ with a smaller mean distance.

The above RDFs are redrawn in Figure 4 to better compare with each other. The cation−cation, cation−anion, and anion−anion RDFs are arranged to be in the first, second, and third rows, respectively, and the first column is at 500 K, and the second column is at 700 K. In all of the plots, solid lines correspond to $[EMI^+][BF_4^-]$, and dashed lines are $[VIO^{2+}]$-$[BF_4^-]_2$. The $[VIO^{2+}][BF_4^-]_2$ cation−cation RDFs have an apparent shift to a larger distance with respect to $[EMI^+][BF_4^-]$ at both temperatures, which can be understood by the difference in molecular size and shape. At T = 500 K, a small bump appears at 0.45 nm for $[EMI^+][BF_4^-]$ and at 0.6 nm for $[VIO^{2+}][BF_4^-]_2$. At T = 700 K in Figure 4b, the bump still presents for the latter but disappears for the former. Similar bumps in the cation−cation RDF were previously observed by Yan and co-workers[52] for the 1-ethyl-3-methyl-imidazolium nitrate ($[EMI^+][NO_3^-]$) IL and were interpreted as the consequence of the cation alignment.

The $[VIO^{2+}][BF_4^-]_2$ IL has a sharper $g_{+-}(r)$ main peak than $[EMI^+][BF_4^-]$ at both temperatures. In addition, a small bump presents at 0.7 nm before the first valley for $[VIO^{2+}][BF_4^-]_2$. Interestingly, this bump is at a position slightly utmost than the bump formed in the cation−cation RDF, suggesting a correlation between this bump and that observed in $g_{++}(r)$. The $g_{--}(r)$ for both ILs differ in the ordering of anions. As shown in Figure 4e, the first peak of the $[VIO^{2+}][BF_4^-]_2$ anion−anion RDF is located at a smaller distance and is higher and sharper than $[EMI^+][BF_4^-]$, indicating that the anions are packed more closely due to the larger positive charges of $[VIO^{2+}]$. Consequently, the $g_{--}(r)$ of $[VIO^{2+}][BF_4^-]_2$ damps faster than that of $[EMI^+][BF_4^-]$. The above RDF results indicate that the dicationic nature of the methyl-viologen cation results in closer-packed anions with a stronger correlation with cations.

As described in the Introduction section, to distinguish the effect of the rigidity and the dicationicity of $[VIO^{2+}]$, we further simulated two artificially modified IL systems. The first one is a viologen-based IL with the constraint keeping the two cationic rings in the same plane turned off, and the second one has the total partial charge of $[VIO^{2+}]$ rescaled to be +1. Both have $[BF_4^-]$ as the anion. We present in Figure 5 the RDFs for the first modified system compared with the RDFs of the original system as well as the $[EMIM^+][BF_4^-]$ system. The cationic flexibility allows cations to come closer (panels a and b) and the

DOI: 10.1021/acs.jpcb.6b03379
J. Phys. Chem. B 2016, 120, 5678−5690

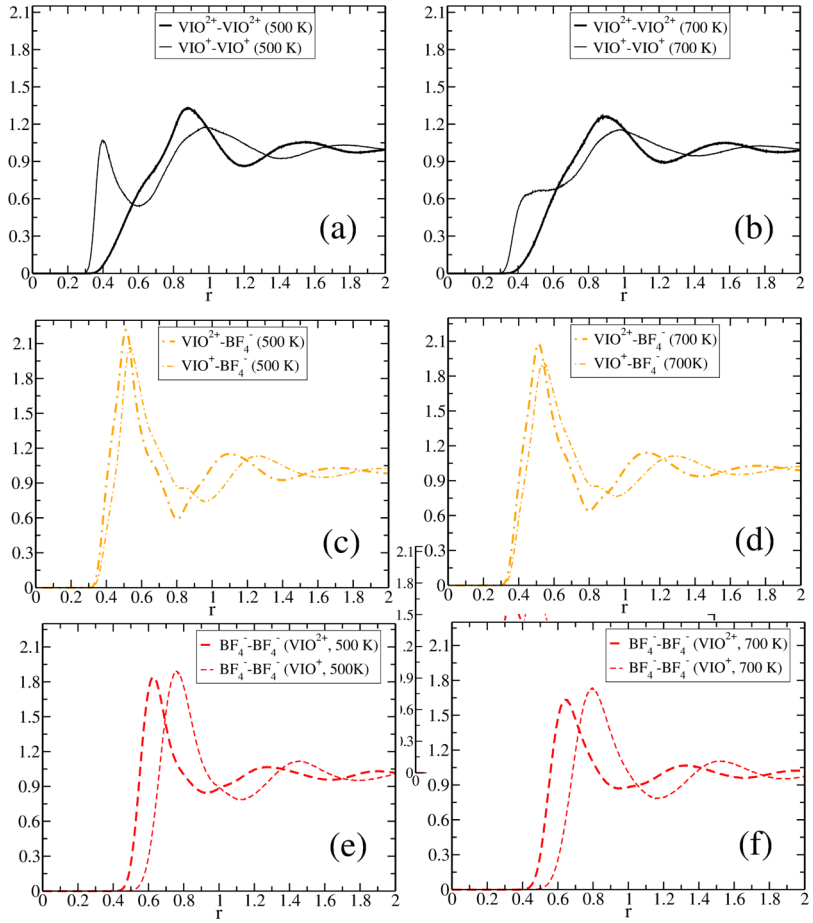

Figure 6. Comparison of the RDFs for the $[VIO^+]$ $[BF_4^-]$ system with the $[VIO^{2+}]$ $[BF_4^-]_2$ system. The left column shows the results at T = 500 K, and the right column is at T = 700 K. The first, second, and third rows show cation−cation, cation−anion, and anion−anion RDFs, respectively.

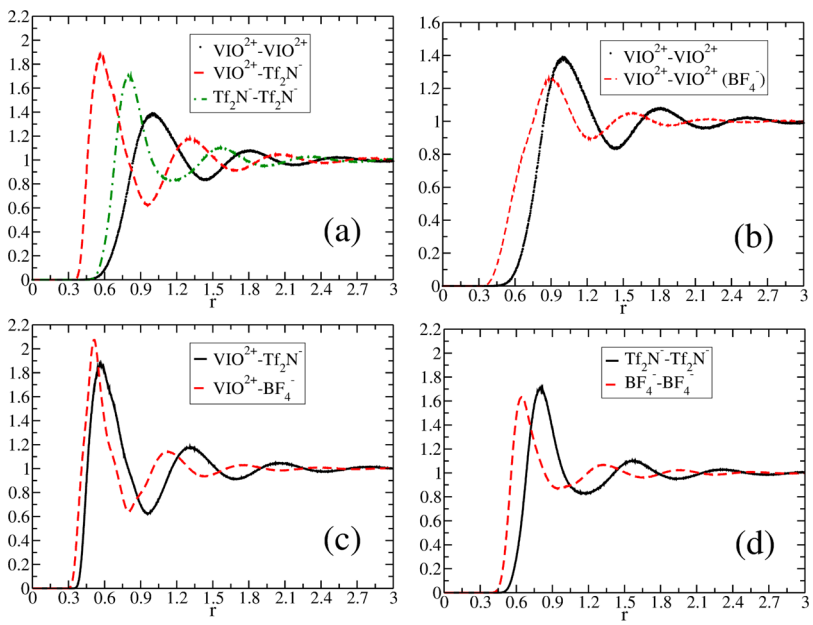

Figure 7. RDFs for $[VIO^{2+}][Tf_2N^-]_2$ at T = 700 K (a) and comparisons of cation−cation (b), cation−anion (c), and anion−anion (d) RDFs between $[VIO^{2+}][Tf_2N^-]_2$ and $[VIO^{2+}][BF_4^-]_2$.

principal peak on the cation−anion RDF to slightly shift to a shorter distance (panels c and d), but the anion−anion RDFs remain unchanged (panels e and f). Figure 6 show the results for the second modified system compared with the original system. All RDFs shift to the right when the cationic partial charge is reduced, indicating a reduction of ionic correlations

DOI: 10.1021/acs.jpcb.6b03379
J. Phys. Chem. B 2016, 120, 5678−5690

induced by electrostatic interactions. In particular, the first peak of the anion−anion RDF shifts more than one Angstrom. From the above results, we conclude that the rigidity of the $[VIO^{2+}]$ cation has a marginal effect on the structural properties.

In order to explore the effect of anion flexibility, we have additionally performed MD simulations for dimethylviologen bistriflimide at T = 700 K. The COM-RDFs were employed to quantify the structural properties. The COM-RDFs of $[VIO^{2+}][BF_4^-]_2$ and $[VIO^{2+}][Tf_2N^-]_2$ are plotted in Figure 7a−d. We can see in Figure 7a that the main peak positions of $g_{++}(r)$ and $g_{--}(r)$ do not coincide with the first minimum position of $g_{+-}(r)$. A more detailed comparison shown in Figure 7b indicates that the bump at around 0.45 nm presented in the $[VIO^{2+}][BF_4^-]_2$ cation−cation RDF disappears for $[VIO^{2+}][Tf_2N^-]_2$. In Figure 7c, we can see two essential differences: the $[VIO^{2+}][BF_4^-]_2$ cation−anion RDF has a sharper main peak and a bump at around 0.7 nm. In Figure 7d, we can see the shift to a larger distance of the anion−anion RDF for $[VIO^{2+}][Tf_2N^-]_2$. On the basis of those results, we conclude that (1) the screening scheme for both ILs is similar; (2) the cations of $[VIO^{2+}][Tf_2N^-]_2$ no longer align; and that (3) for $[VIO^{2+}][Tf_2N^-]_2$, a similar anion structure shifts to a larger distance due to the larger size of the bistriflimide anion.

3.2. Static Orientational Order Parameter. It was found that the emergence of a bump in the cation−cation RDF may relate to a certain rotational ordering.[52] To understand the bumps appearing in the RDFs, we have further calculated the static orientational order parameter (SOP) $P_2[\theta(r)]$ defined in eq 1, whose results are shown in Figure 8. We can see that the

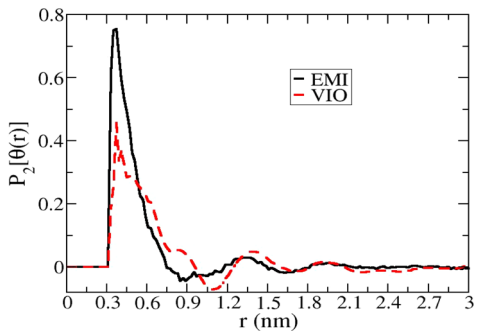

Figure 8. Static orientational order parameter[16] $P_2[\theta(r)]$ as a function of the distance at T = 500 K. The result for $[EMI^+][BF_4^-]$ is plotted with a solid line, and the dashed line is for $[VIO^{2+}][BF_4^-]_2$.

SOP has a significant peak at 0.45 nm for $[EMI^+]$ and at 0.6 nm for $[VIO^{2+}]$ and otherwise is close to zero. According to the SOP definition, the first peaks can be interpreted as the alignment of the adjacent cationic ring planes. For both ILs, the RDF bumps and the SOP peaks are at the same locations, indicating that the bumps in the cation−cation RDFs come from the ring alignment of adjacent cations.

Next, we present in Figure 9a−d an illustration of the cation alignment. Figure 9a and b shows the snapshots in which aligned cations are depicted as solid molecules and the rest as transparent molecules. Figure 9c and d illustrates a pair of viologen and imidazolium cations, respectively. We can see that the distance between the center of mass of both cations is smaller for aligned cations. In addition, we observe the anions appearing beside the cationic rings rather than in between. This kind of cationic alignment certainly serves as the precursor of a crystal structure in these ILs.

The small bump at 0.7 nm in the $[VIO^{2+}][BF_4^-]_2$ $g_{+-}(r)$ is a consequence of the fact that anions present at the side of cationic rings. Interestingly, the $g_{+-}(r)$ of $[EMI^+][BF_4^-]$ does not present a bump between the first and second peaks because the EMI^+ cations allow anions to stay as close as inside the first coordination shell.

3.3. Radial Distribution Functions between Anions and Hydrogen Atoms. As described above, the most important difference between the two studied IL systems is the local ordering of the $[BF_4^-]$ anions. In order to obtain a better understanding of the detailed microscopic molecular structures, we have calculated the RDFs of anions with respect to various cationic hydrogen atoms. As shown in the inset of Figure 10a, for $[EMI^+][BF_4^-]$, the hydrogen atoms are labeled as H5, H4, H1, and HC. The H5 and H4 hydrogen atoms are on the imidazolium ring, the H1 is in the methyl-group, and the HC atom is associated with the ethyl chain. The RDFs shown in Figure 10a indicate that the mean distance is almost identical for the four hydrogen types, and a high concentration of anions is around the H5 atom due to its relatively large partial charge. In contrast, HC exhibits a lower mean peak, indicating a poor affinity of anions with the ethyl groups.

However, the $[VIO^{2+}][BF_4^-]_2$ ILs have three kinds of hydrogen atoms: H4 and HA are bonded to the viologen rings, and H1 is bonded to the external methyl groups. Figure 10b shows the anion RDFs around the viologen hydrogens, whose first peak positions are almost identical. In addition, the H1-BF_4 and H4-BF_4 RDFs have similar main peak heights higher than the HA-BF_4 RDF. The coincidence of the main peak positions indicates that the anionic average shell takes an ellipsoidal shape induced by the rod-like form of the viologen molecule. However, the anions prefer to associate with the external part of the VIO^{2+} rings. This preference can be understood by taking into account the fact that most positive partial charges concentrate on the external parts of the viologen cationic rings, which attract anions to stay around this region most of the time.

3.4. Spatial Distribution Functions. The spatial distribution functions (SDFs) are shown in Figures 11a−d. We can observe in Figure 11a a first coordination shell composed of anions and surrounded by a second shell mainly formed by cations, consistent with Figure 3a. In agreement with Figure 10a, the anions concentrate around H5 and H4. In Figure 11b, the $[BF_4^-]$ SDF shows that the anion is surrounded mainly by cations in the first coordination shell and that the second shell is formed by anions. Because of the structural symmetry in the $[BF_4^-]$ molecule, the average ionic distribution maintains a quasi-spherical symmetry.

Figures 11c and d present the SDF for $[VIO^{2+}][BF_4^-]_2$. Figure 11c shows an inner shell of anions surrounded by a shell of cations. A high occupation of anions is around the H4 atoms at the outer side of the viologen rings, consistent with Figures 3c and 10b. In Figure 11d, we can see that a compact structure composed of cations and anions surrounds the central anion, in good agreement with Figures 3a,b and 4c,e.

3.5. Summary of Structural Properties. We have observed that anions of $[VIO^{2+}][BF_4^-]_2$ tend to form a close-packed ordering due to the dicationic nature of the methyl-viologen molecule but that the anions around $[EMI^+]$ have a longer range correlation. The viologen molecule promotes a close-packed local structure instead of the long-range ordering found in the monocationic IL. This difference can be understood by considering the competition between two

DOI: 10.1021/acs.jpcb.6b03379
J. Phys. Chem. B 2016, 120, 5678−5690

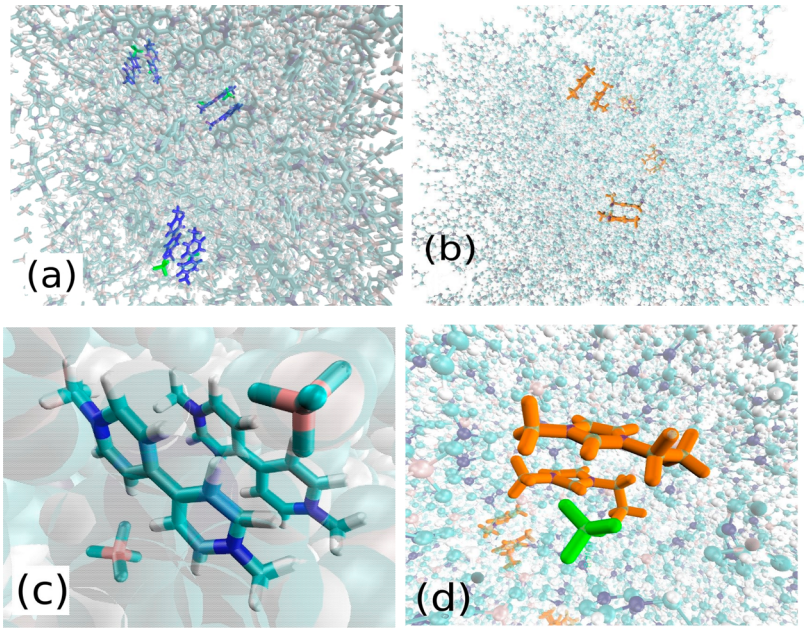

Figure 9. Illustration of the alignment of the imidazolium and viologen cations. (a and b) Randomly chosen snapshots in which aligned cations are depicted as solid molecules and the rest of the system as transparent molecules. (c and d) A pair of viologen and imidazolium cations, respectively, with the anions accommodated at the side of the cations.

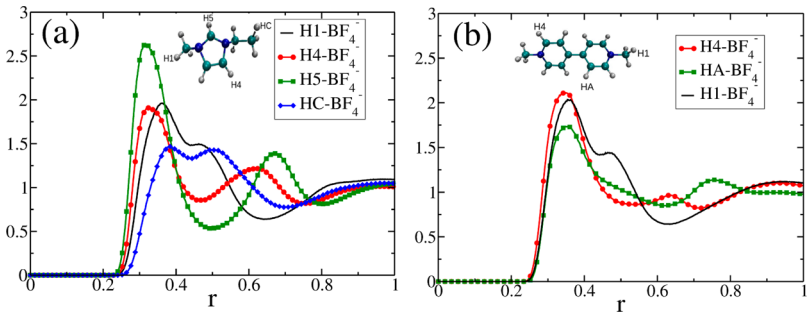

Figure 10. Hydrogen-anion radial distribution functions for $[EMI^+][BF_4^-]$ (a) and $[VIO^{2+}]$ $[BF_4^-]_2$ (b). The H1-BF_4 RDFs are drawn with black lines, H4-BF_4 RDF red lines with circles, H5-BF_4 RDF green lines with squares, and HC-BF_4 RDF blue line with diamonds.

factors: the inhomogeneous charge distribution of $[EMI^+]$ prefers a loose structure of anions, and the large positive partial charge taken by $[VIO^{2+}]$ promotes a compact structure of anions around its two rings. A little bump appears in the cation−cation RDFs of both ILs due to the alignment of cation rings. The anion distributions around cations are also different by another small bump before the first valley of the cation−anion RDF for $[VIO^{2+}][BF_4^-]_2$ due to the occupancy of anions beside the aligned cations.

Our results for $[EMI^+][BF_4^-]$ are analogous to the MD results by Li and co-workers[41] for monocationic imidazolium-based ILs. However, several differences can be found for $[VIO^{2+}][BF_4^-]_2$ on the ordering of ions linked to the additional interaction sites on the two viologen rings: eight rather than six hydrogen bonding sites are on each cation. Another important source of differences is the rigidity of the bypiridinium core in contrast with the flexibility of di-imidazolium cations. Unlike the imidazolium dications studied in ref 44, which can bend due to the flexibility of the alkyl chain, the bipyridinium core cannot bend; as a result, the viologen cations are difficult to rotate even at high temperatures.

4. RESULTS: DYNAMICAL PROPERTIES

4.1. Mean Square Displacements. The calculated mean square displacements (MSDs) at T = 500 and 700 K for the two IL systems are presented in Figure 12a and b. In both panels, bold lines are for $[EMI^+][BF_4^-]$ and thin lines for $[VIO^{2+}][BF_4^-]_2$. Solid and dashed lines represent cations and anions, respectively.

As expected, both systems exhibit a ballistic regime in a short time followed by a plateau and finally a linear regime. Notice that $[BF_4^-]$ has a slightly smaller MSD slope than $[EMI^+]$ at both temperatures, in good agreement with the previous MD results for imidazolium-based ILs.[55] However, we can observe a slower diffusivity for $[VIO^{2+}][BF_4^-]_2$. As listed in Table 2, the diffusion coefficient of $[VIO^{2+}][BF_4^-]_2$ is about 2 orders of magnitude less than $[EMI^+][BF_4^-]$ at 500 K and 1 order of magnitude at 700 K.

As shown in Figure 12b, the viologen cation decreases the system mobility. Interestingly, anions diffuse slightly slower than cations in $[EMI^+][BF_4^-]$ but slightly faster in $[VIO^{2+}]$-$[BF_4^-]_2$. The modified systems first described in the Introduction section were used again to probe the effect of the rigidity and total charge on system dynamics. The

DOI: 10.1021/acs.jpcb.6b03379
J. Phys. Chem. B 2016, 120, 5678−5690

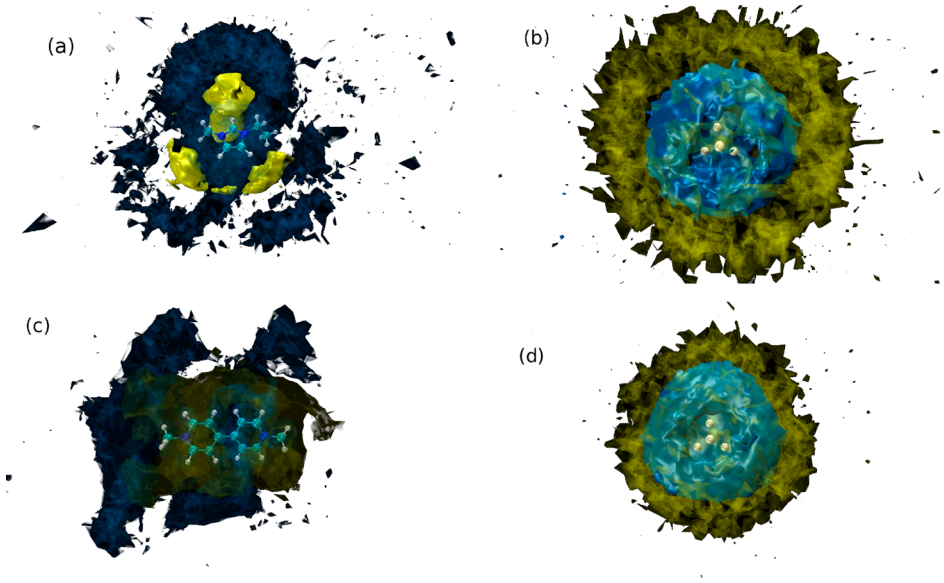

Figure 11. Spatial distribution function for the ions at T = 500 K. The blue surface corresponds to the cation distribution, and yellow is anion distribution. The first column shows the average distribution around cations, while the right column shows the accommodation around anions. Panel a shows the inhomogeneous distribution of anions around the most charged hydrogens of the [EMI$^+$] cation. In contrast, as shown in panel b, the distribution around the anion is very symmetric. Panel c clearly shows that the anions concentrate around the two rings of [VIO^{2+}]. Panel d shows a closed packed distribution around the anion for [VIO^{2+}][BF$_4^-$]$_2$. The images were created with VMD.[54]

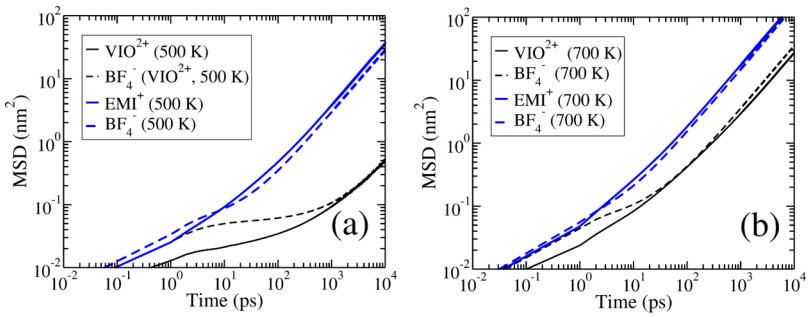

Figure 12. MSDs for the imidazolium- and viologen-based ILs at (a) 500 K and (b) 700 K. Solid lines are for cations, and dashed lines are for anions. The blue lines are for [EMI$^+$][BF$_4^-$], and the black lines are for [VIO^{2-}][BF$_4^-$]$_2$.

Table 2. Diffusion Coefficients for [VIO^{2+}][BF$_4^-$]$_2$ and [EMI$^+$][BF$_4^-$][a]

ion	T (K)	D ($\times 10^{-5}$ cm^2/s)
EMI$^+$	500	0.598 (±0.0366)
BF$_4^-$ (EMI$^+$)	500	0.4732 (±0.0088)
VIO^{2+}	500	0.0064 (±0.0016)
BF$_4^-$ (VIO^{2+})	500	0.007 (±0.0013)
EMI$^+$	700	2.867 (±0.1198)
BF$_4^-$ (EMI$^+$)	700	2.579 (±0.0047)
VIO^{2+}	700	0.4525 (±0.0049)
BF$_4^-$ (VIO^{2+})	700	0.5869 (±0.0107)

[a]The first four rows are the results at T = 500 K, and the other four are at T = 700 K.

comparison with the modified system with a flexible [VIO^{2+}] cation is shown in Figure 13a and b. The ion mobility increases when the cation becomes flexible, demonstrating that cationic rigidity greatly obstacles ion diffusion. In addition, the dicationic nature of viologen also has a significant impact on system diffusion. Figure 14a and b shows that the dicationic IL is less mobile than the one with reduced charge, whose mobility is very similar to that of the imidazolium-based IL.

To study the effect of anion flexibility on system dynamics, the MSDs of [VIO^{2+}][BF$_4^-$]$_2$ and [VIO^{2+}][Tf$_2$N$^-$]$_2$ have been calculated and are presented in Figure 15. We can see that both ILs have almost the same cationic MSDs but that [Tf$_2$N$^-$] anions diffuse slower than [BF$_4^-$] due to their larger size. Therefore, we conclude that replacing anion species does not significantly alter the dynamic properties of viologen cations.

4.2. Rotational Autocorrelation Function. The cation RACFs have been calculated according to eq 2 and are plotted in Figure 16a and b. As shown in Figure 16a, the RACF at 500 K is slow for both cations. The imidazolium RACF requires about 100 ps to relax, and the viologen RACF presents a large plateau that extends about 5 orders of magnitude longer in time than the imidazolium. The RACFs at 700 K, shown in Figure 16b, are faster than that at 500 K, but the viologen still requires about 500 ps to relax. Therefore, we conclude that the [VIO^{2+}] cations are always more difficult to rotate than [EMI$^+$] and that the former prefer to remain aligned for a longer time than the latter. The large difference in the RACFs can be understood by the rigid rod-like form of the [VIO^{2+}] cation which requires that both pyridinium rings rotate simultaneously. In contrast, the imidazolium cation only has to rotate a single ring. Therefore, rigidity is vital in slowing down the rotational

DOI: 10.1021/acs.jpcb.6b03379
J. Phys. Chem. B 2016, 120, 5678−5690

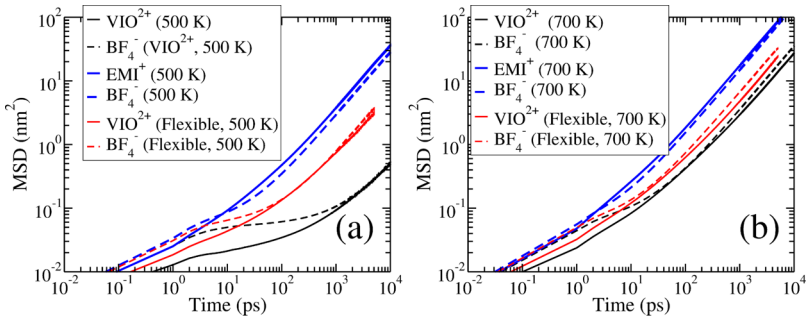

Figure 13. MSDs of the modified system with a flexible dication compared to the original system as well as $[EMI^+][BF_4^-]$ at T = 500 K (a) and T = 700 K (b).

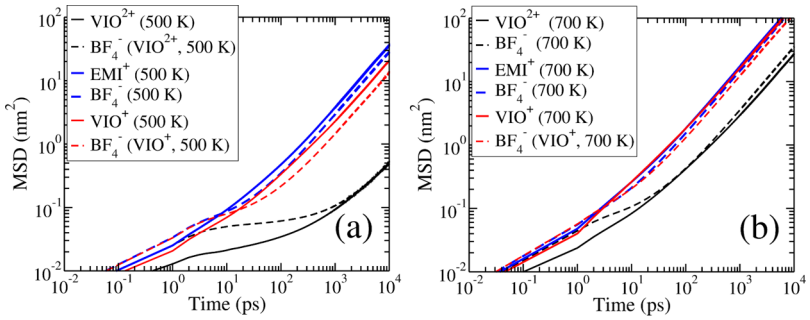

Figure 14. MSDs of the modified system with reduced cationic charges compared to the original system as well as $[EMI^+][BF_4^-]$ at T = 500 K (a) and T = 700 K (b).

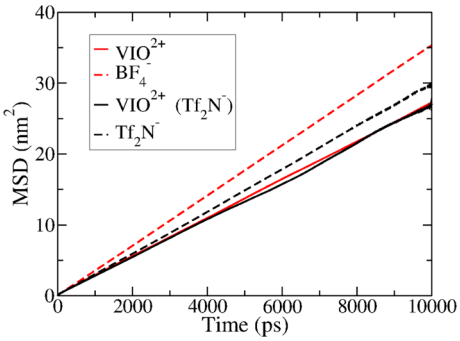

Figure 15. MSDs of $[VIO^{2+}][Tf_2N^-]_2$ and $[VIO^{2+}][BF_4^-]_2$ ILs at T = 700 K.

motion of the dimethyl-viologen cation inside a highly structured ion cage.

4.3. Ion-Cage Lifetime. In order to quantify the long lifetime of the ion cages, we have calculated the ion-cage correlation (ICC) defined in eq 3. Figure 17a and b shows the time dependence of the ICC for both ILs. In Figure 17a, we can observe a very slow decay of the ICC at 500 K. For the $[EMI^+][BF_4^-]$ IL, the ICC relaxes in a time window of 3 ns, but the $[VIO^{2+}][BF_4^-]_2$ ions remain paired for more than 4 ns. A similar scenario is observed in our simulations at T = 700 K presented in Figure 17b, in which the relaxation of $[EMI^+]$-$[BF_4^-]$ is still faster than $[VIO^{2+}][BF_4^-]_2$.

Our results suggest that using a dication instead of a monocation has a great influence on the stability of the ion cage because the stronger electrostatic interaction increases the stability of ion pairs, and the rigidity of the bipyridinium cation increases at a lower temperature. Clearly, a rigid large cation stabilizes the ion cage due to the slower translational and rotational diffusions, which leads to a long ion-pair lifetime because the anions are effectively trapped between the cations. Our results provide additional support to the importance of the recently discovered ion-cage effect[56] on the dynamic and transport properties of ILs.

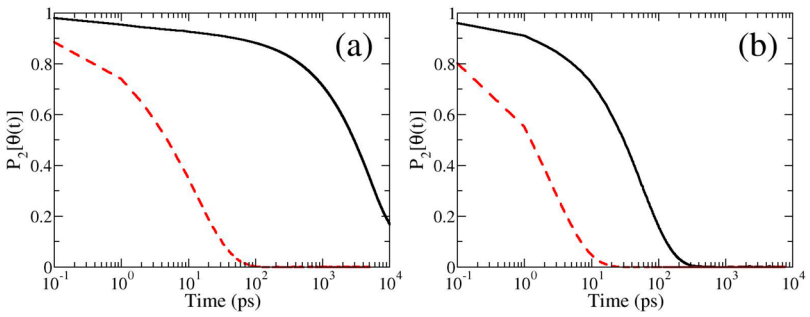

Figure 16. Rotational autocorrelation function for the cations of $[VIO^{2+}][BF_4^-]_2$ (solid lines) and $[EMI^+][BF_4^-]$ (dashed lines) at T = 500 K (a) and 700 K (b).

DOI: 10.1021/acs.jpcb.6b03379
J. Phys. Chem. B 2016, 120, 5678−5690

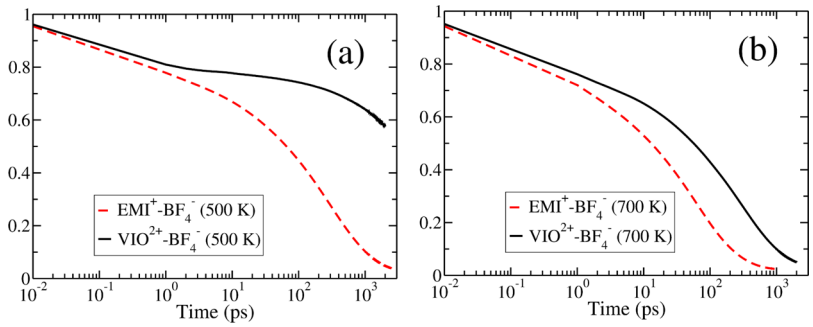

Figure 17. Ion-cage correlation function for $[EMI^+][BF_4^-]$ (dashed lines) and $[VIO^{2+}][BF_4^-]_2$ (solid lines) at (a) 500 K and (b) 700 K.

4.4. Summary of Dynamical Properties. We have observed that all the dynamical correlation functions of $[VIO^{2+}][BF_4^-]_2$ present a slower relaxation than $[EMI^+][BF_4^-]$ at both T = 500 and 700 K. The MSD shows that $[EMI^+][BF_4^-]$ has a faster diffusion and that its anions diffuse slower than the cations. For $[VIO^{2+}][BF_4^-]_2$, both cations and anions present a very slow mobility. At 700 K, the diffusion increases for both ILs, but $[VIO^{2+}][BF_4^-]_2$ is still slower.

The RACF shows that the rotational diffusion of $[VIO^{2+}][BF_4^-]_2$ is very difficult at both temperatures due to the rigidity of the viologen cation. We have shown that the slowing down of the dynamical properties can be understood by the long-living ion-cage effect, which is more significant for $[VIO^{2+}][BF_4^-]_2$. On the basis of the structural differences previously described, we can conclude that the slowing down of the $[VIO^{2+}][BF_4^-]_2$ diffusion (translational and rotational) can be understood by the dicationic nature and the rigidity of the $[VIO^{2+}]$ cation. Of course, the large size difference between the cation and the anion also contribute to the difference in diffusion since the long-distance electrostatic interactions allow small molecules to diffuse in available spaces, but the large rod-like viologen cation has no enough space to easily move, and the combination of electrostatic and nonoverlapping interactions reduce the possibility of an efficient diffusion in this system. Nevertheless, a more important factor is the two positive charges on the methyl-viologen cation which force the anions to be close-packed with the cations to maintain an efficient local neutrality, and they are hard to diffuse. In addition, the close-packed local structure slows down the cationic diffusion because the ion cage surrounding the cations has a longer lifetime.

Finally, the rigidity of the viologen cations does not permit the anions to move in an efficient way and thus slows down the diffusion of all ions in the system. In addition, the rigidity is a prominent obstacle for the rotational diffusion of the viologen cation, which requires the two rings to rotate together.

5. CONCLUSIONS

In this work, MD simulations were employed to perform a systematic comparison between the monocationic IL $[EMI^+][BF_4^-]$, the dicationic IL $[VIO^{2+}][BF_4^-]_2$, and $[VIO^{2+}][Tf_2N^-]_2$ to study the influence of molecular flexibility on the structural and dynamical properties of ILs. For the structural properties, the RDFs and SDFs reveal that the local ordering of anions is different. The anions in $[VIO^{2+}][BF_4^-]_2$ are close packed and highly correlated to the viologen rings, in particular to the external part of the cation. For the cations in both ILs, the orientational order parameter $P_2[(r)]$ shows a strong tendency of parallel alignment, corresponding to the bumps in the cation−cation RDFs of $[EMI^+][BF_4^-]$ and $[VIO^{2+}][BF_4^-]_2$, which, along with the close-packed structures, might be a precursor toward crystallization. The bumps disappear for $[VIO^{2+}][Tf_2N^-]_2$ because the $[Tf_2N^-]$ anions have a larger exclusive volume and introduce a larger degree of disordering due to their flexibility. Our results can also explain the drastic decrease of the melting temperature when rigid anions, such as halides, are replaced by bistriflimide anions.

The dynamics of $[VIO^{2+}][BF_4^-]_2$ is slower than $[EMI^+][BF_4^-]$, even at high temperatures. Besides the general slowing down in diffusion, we have also found that, for $[VIO^{2+}][BF_4^-]_2$, the anions are always more mobile than the cations, which is not the case for $[EMI^+][BF_4^-]$. The cationic dynamics is not affected by different anions. Moreover, we have found that the ion cage of $[VIO^{2+}][BF_4^-]_2$ is more stable, responsible for the main differences between the dynamic behavior of both ILs. The stability of the ion-cage can be attributed to the dicationic nature and the rigidity of the $[VIO^{2+}]$ cation.

We have identified two factors responsible for the main differences between both ILs. The first reason is the dicationic versus the monocationic nature of the cations. The two charges in the methyl-viologen molecule promote a higher correlation between its rings and the anions. This strong correlation is due to the tendency of Coulombic fluids to establish local neutrality on average. Consequently, the viologen cation always requires two anions to compensate its positive two charges, promoting a stronger and close-packed local structure. The second reason is the rigidity of the bipyridinium cation compared with the flexible imidazolium molecule.[57] The flexibility plays a fundamental role in the rotational motion and the alignment of cations. The usage of a more flexible anion, such as $[VIO^{2+}][Tf_2N^-]_2$, destroys the cation alignment and makes the isotropic phase more favorable

We further verified our interpretations by simulating two modified viologen-based ILs. The results for the first one with the rigidity of the viologen cation turned off indicate that the introduction of flexibility only slightly affects the structural properties but significantly increases the system mobility. The results for the second one with the total cationic charge reduced from +2 to +1 indicate that the cationic charge has a great influence on both structural and dynamical properties: the intermolecular structure becomes looser, and the system diffusion increases, both of which can be attributed to the decrease of attractive electrostatic interaction between cations and anions.

Finally, we would like to emphasize the fact that the rigid and dicationic nature of $[VIO^{2+}]$ has a significant impact on the phase behavior of corresponding ILs. Despite the fact that we have studied both ILs in the liquid phase, it is natural to

DOI: 10.1021/acs.jpcb.6b03379
J. Phys. Chem. B 2016, 120, 5678−5690

conceive that the strong correlations of anions and the tendency of cations to align are indicative of a higher preference of the crystalline structure for $[VIO^{2+}][BF_4^-]_2$ than $[EMI^+][BF_4^-]$ because the two charged cationic rings promote a strong correlation and a spatial ordering of the anions.

■ AUTHOR INFORMATION

Corresponding Author

*Phone: +86 10-62648749. E-mail: wangyt@itp.ac.cn.

Notes

The authors declare no competing financial interest.

■ ACKNOWLEDGMENTS

This work was supported by the National Basic Research Program of China (973 program, No. 2013CB932804) and the National Natural Science Foundation of China (Nos. 11274319 and 11421063). The computations of this work were conducted on the HPC cluster of ITP-CAS and the supercomputer of SCCAS. We also thank the CNR-CAS 2014-2016 bilateral agreement for support.

■ REFERENCES

(1) Freyland, W. *Coulombic Fluids*; Springer Series in Solid-State Sciences; Springer: Berlin, Germany, 2011; Vol. *168*.

(2) Hansen, J.-P.; McDonald, I. R. *Theory of Simple Liquids: With Applications to Soft Matter*; Academic Press: New York, 2013.

(3) Mamantov, G., Marassi, R., Eds. *Molten Salt Chemistry*; Springer: Dordrecht, The Netherlands, 1987.

(4) Welton, T. Room-Temperature Ionic Liquids. Solvents for Synthesis and Catalysis. *Chem. Rev.* **1999**, *99* (8), 2071−2084.

(5) Wasserscheid, P.; Welton, T. *Ionic Liquids in Synthesis*, 2nd ed.; Wiley: New York. http://www.wiley.com/WileyCDA/WileyTitle/productCd-3527312390.html (accessed Mar 12, 2016).

(6) Rogers, R. D. CHEMISTRY: Ionic Liquids–Solvents of the Future? *Science* **2003**, *302* (5646), 792−793.

(7) Plechkova, N. V.; Seddon, K. R. Applications of Ionic Liquids in the Chemical Industry. *Chem. Soc. Rev.* **2008**, *37* (1), 123−150.

(8) Gale, R. J.; Gilbert, B.; Osteryoung, R. A. Raman Spectra of Molten Aluminum Chloride: 1-Butylpyridinium Chloride Systems at Ambient Temperatures. *Inorg. Chem.* **1978**, *17* (10), 2728−2729.

(9) Wilkes, J. S.; Zaworotko, M. J. Air and Water Stable 1-Ethyl-3-Methylimidazolium Based Ionic Liquids. *J. Chem. Soc., Chem. Commun.* **1992**, *13*, 965.

(10) Monk, P. M. S. *The Viologens: Physicochemical Properties, Synthesis, and Applications of the Salts of 4,4′-bipyridine*; Wiley: New York, 1998.

(11) Jordão, N.; Cabrita, L.; Pina, F.; Branco, L. C. Novel Bipyridinium Ionic Liquids as Liquid Electrochromic Devices. *Chem. - Eur. J.* **2014**, *20* (14), 3982−3988.

(12) Tabushi, I.; Yamamura, K.; Kominami, K. Electric Stimulus-Response Behavior of Liquid-Crystalline Viologen. *J. Am. Chem. Soc.* **1986**, *108* (20), 6409−6410.

(13) Yamamura, K.; Okada, Y.; Ono, S.; Kominami, K.; Tabushit, I. New Liquid Crystalline Viologens Exhibiting Electric Stimulus-Response Behavior. *Tetrahedron Lett.* **1987**, *28* (51), 6475−6478.

(14) Hatazawa, T.; Terrill, R. H.; Murray, R. W. Microelectrode Voltammetry and Electron Transport in an Undiluted Room Temperature Melt of an Oligo(ethylene Glycol)-Tailed Viologen. *Anal. Chem.* **1996**, *68* (4), 597−603.

(15) Haramoto, Y.; Yin, M.; Matukawa, Y.; Ujiie, S.; Nanasawa, M. A New Ionic Liquid Crystal Compound with Viologen Group in the Principal Structure. *Liq. Cryst.* **1995**, *19* (3), 319−320.

(16) Binnemans, K. Ionic Liquid Crystals. *Chem. Rev.* **2005**, *105* (11), 4148−4204.

(17) Axenov, K. V.; Laschat, S. Thermotropic Ionic Liquid Crystals. *Materials* **2011**, *4* (12), 206−259.

(18) Pibiri, I.; Pace, A.; Buscemi, S.; Causin, V.; Rastrelli, F.; Saielli, G. Oxadiazolyl-Pyridines and Perfluoroalkyl-Carboxylic Acids as Building Blocks for Protic Ionic Liquids: Crossing the Thin Line between Ionic and Hydrogen Bonded Materials. *Phys. Chem. Chem. Phys.* **2012**, *14* (41), 14306.

(19) Bhowmik, P. K.; Han, H.; Cebe, J. J.; Burchett, R. A.; Acharya, B.; Kumar, S. Ambient Temperature Thermotropic Liquid Crystalline Viologen Bis(triflimide) Salts. *Liq. Cryst.* **2003**, *30* (12), 1433−1440.

(20) Bhowmik, P.; Han, H.; Nedeltchev, I.; Cebe, J. Room-Temperature Thermotropic Ionic Liquid Crystals: Viologen Bis-(Triflimide) Salts. *Mol. Cryst. Liq. Cryst.* **2004**, *419* (1), 27−46.

(21) Causin, V.; Saielli, G. Effect of Asymmetric Substitution on the Mesomorphic Behaviour of Low-Melting Viologen Salts of Bis-(trifluoromethanesulfonyl)amide. *J. Mater. Chem.* **2009**, *19* (48), 9153.

(22) Causin, V.; Saielli, G. Effect of a Structural Modification of the Bipyridinium Core on the Phase Behaviour of Viologen-Based Bistriflimide Salts. *J. Mol. Liq.* **2009**, *145* (1), 41−47.

(23) Bonchio, M.; Carraro, M.; Casella, G.; Causin, V.; Rastrelli, F.; Saielli, G. Thermal Behaviour and Electrochemical Properties of Bis(trifluoromethanesulfonyl)amide and Dodecatungstosilicate Viologen Dimers. *Phys. Chem. Chem. Phys.* **2012**, *14* (8), 2710.

(24) Casella, G.; Causin, V.; Rastrelli, F.; Saielli, G. Viologen-Based Ionic Liquid Crystals: Induction of a Smectic A Phase by Dimerisation. *Phys. Chem. Chem. Phys.* **2014**, *16* (11), 5048.

(25) Tokuda, H.; Hayamizu, K.; Ishii, K.; Susan, M. A. B. H.; Watanabe, M. Physicochemical Properties and Structures of Room Temperature Ionic Liquids. 2. Variation of Alkyl Chain Length in Imidazolium Cation. *J. Phys. Chem. B* **2005**, *109* (13), 6103−6110.

(26) Abraham, M. A.; Moens, L. Clean Solvents. Alternative Media for Chemical Reactions and Processing. *J. Am. Chem. Soc.* **2003**, *125* (3), 850−850.

(27) Huddleston, J. G.; Visser, A. E.; Reichert, W. M.; Willauer, H. D.; Broker, G. A.; Rogers, R. D. Characterization and Comparison of Hydrophilic and Hydrophobic Room Temperature Ionic Liquids Incorporating the Imidazolium Cation. *Green Chem.* **2001**, *3* (4), 156−164.

(28) Wakai, C.; Oleinikova, A.; Ott, M.; Weingärtner, H. How Polar Are Ionic Liquids? Determination of the Static Dielectric Constant of an Imidazolium-Based Ionic Liquid by Microwave Dielectric Spectroscopy. *J. Phys. Chem. B* **2005**, *109* (36), 17028−17030.

(29) Bonhôte, P.; Dias, A.-P.; Papageorgiou, N.; Kalyanasundaram, K.; Grätzel, M. Hydrophobic, Highly Conductive Ambient-Temperature Molten Salts †. *Inorg. Chem.* **1996**, *35* (5), 1168−1178.

(30) Lee, K. M.; Lee, C. K.; Lin, I. J. B. First Example of Interdigitated U-Shape Benzimidazolium Ionic Liquid Crystals. *Chem. Commun.* **1997**, *9*, 899−900.

(31) Gordon, C. M.; Holbrey, J. D.; Kennedy, A. R.; Seddon, K. R. Ionic Liquid Crystals: Hexafluorophosphate Salts. *J. Mater. Chem.* **1998**, *8* (12), 2627−2636.

(32) Holbrey, J. D.; Seddon, K. R. The Phase Behaviour of 1-Alkyl-3-Methylimidazolium Tetrafluoroborates; Ionic Liquids and Ionic Liquid Crystals. *J. Chem. Soc., Dalton Trans.* **1999**, *13*, 2133−2140.

(33) Lee, C. K.; Huang, H. W.; Lin, I. J. B. Simple Amphiphilic Liquid Crystalline N-Alkylimidazolium Salts. A New Solvent System Providing a Partially Ordered Environment. *Chem. Commun.* **2000**, *19*, 1911−1912.

(34) Urahata, S. M.; Ribeiro, M. C. C. Single Particle Dynamics in Ionic Liquids of 1-Alkyl-3-Methylimidazolium Cations. *J. Chem. Phys.* **2005**, *122* (2), 024511.

(35) Margulis, C. J. Computational Study of Imidazolium-Based Ionic Solvents with Alkyl Substituents of Different Lengths. *Mol. Phys.* **2004**, *102* (9−10), 829−838.

(36) Urahata, S. M.; Ribeiro, M. C. C. Structure of Ionic Liquids of 1-Alkyl-3-Methylimidazolium Cations: A Systematic Computer Simulation Study. *J. Chem. Phys.* **2004**, *120* (4), 1855.

(37) Del Pópolo, M. G.; Voth, G. A. On the Structure and Dynamics of Ionic Liquids. *J. Phys. Chem. B* **2004**, *108* (5), 1744−1752.

DOI: 10.1021/acs.jpcb.6b03379
J. Phys. Chem. B 2016, 120, 5678−5690

(38) Canongia Lopes, J. N. A.; Pádua, A. A. H. Nanostructural Organization in Ionic Liquids. *J. Phys. Chem. B* **2006**, *110* (7), 3330−3335.
(39) Habasaki, J.; Ngai, K. L. Heterogeneous Dynamics of Ionic Liquids from Molecular Dynamics Simulations. *J. Chem. Phys.* **2008**, *129* (19), 194501.
(40) Zhang, S.; Shi, R.; Ma, X.; Lu, L.; He, Y.; Zhang, X.; Wang, Y.; Deng, Y. Intrinsic Electric Fields in Ionic Liquids Determined by Vibrational Stark Effect Spectroscopy and Molecular Dynamics Simulation. *Chem. - Eur. J.* **2012**, *18* (38), 11904−11908.
(41) Li, S.; Feng, G.; Bañuelos, J. L.; Rother, G.; Fulvio, P. F.; Dai, S.; Cummings, P. T. Distinctive Nanoscale Organization of Dicationic versus Monocationic Ionic Liquids. *J. Phys. Chem. C* **2013**, *117* (35), 18251−18257.
(42) Wang, Y.; Jiang, W.; Voth, G. A. Spatial Heterogeneity in Ionic Liquids. In *Ionic Liquids IV*; Brennecke, J. F., Rogers, R. D., Seddon, K. R., Eds.; American Chemical Society: Washington, DC, 2007; Vol. *975*, pp 272−307.
(43) Cornell, W. D.; Cieplak, P.; Bayly, C. I.; Gould, I. R.; Merz, K. M.; Ferguson, D. M.; Spellmeyer, D. C.; Fox, T.; Caldwell, J. W.; Kollman, P. A. A Second Generation Force Field for the Simulation of Proteins, Nucleic Acids, and Organic Molecules. *J. Am. Chem. Soc.* **1995**, *117* (19), 5179−5197.
(44) de Andrade, J.; Böes, E. S.; Stassen, H. Computational Study of Room Temperature Molten Salts Composed by 1-Alkyl-3-Methylimidazolium CationsForce-Field Proposal and Validation. *J. Phys. Chem. B* **2002**, *106* (51), 13344−13351.
(45) Woods, R.; Chappelle, R. Restrained Electrostatic Potential Atomic Partial Charges for Condensed-Phase Simulations of Carbohydrates. *J. Mol. Struct.: THEOCHEM* **2000**, *527* (1−3), 149−156.
(46) Frisch, M. J.; Trucks, G. W.; Schlegel, H. B.; Scuseria, G. E.; Robb, M. A.; Cheeseman, J. R.; Montgomery, J. A., Jr.; Vreven, T.; Kudin, K. N.; Burant, J. C.; et al. *Gaussian 03*; Gaussian, Inc.: Wallingford, CT, 2004.
(47) Besler, B. H.; Merz, K. M.; Kollman, P. A. Atomic Charges Derived from Semiempirical Methods. *J. Comput. Chem.* **1990**, *11* (4), 431−439.
(48) Liu, H.; Maginn, E. A Molecular Dynamics Investigation of the Structural and Dynamic Properties of the Ionic Liquid 1-N-Butyl-3-Methylimidazolium Bis(trifluoromethanesulfonyl)imide. *J. Chem. Phys.* **2011**, *135* (12), 124507.
(49) Berendsen, H. J. C.; van der Spoel, D.; van Drunen, R. GROMACS: A Message-Passing Parallel Molecular Dynamics Implementation. *Comput. Phys. Commun.* **1995**, *91* (1−3), 43−56.
(50) Essmann, U.; Perera, L.; Berkowitz, M. L.; Darden, T.; Lee, H.; Pedersen, L. G. A Smooth Particle Mesh Ewald Method. *J. Chem. Phys.* **1995**, *103* (19), 8577.
(51) Zhang, S.; Sun, N.; He, X.; Lu, X.; Zhang, X. Physical Properties of Ionic Liquids: Database and Evaluation. *J. Phys. Chem. Ref. Data* **2006**, *35* (4), 1475.
(52) Yan, T.; Wang, Y.; Knox, C. On the Structure of Ionic Liquids: Comparisons between Electronically Polarizable and Nonpolarizable Models I. *J. Phys. Chem. B* **2010**, *114* (20), 6905−6921.
(53) Edwards, F. G.; Howe, R. A.; Enderby, J. E.; Page, D. I. The Structure of Molten Barium Chloride. *J. Phys. C: Solid State Phys.* **1978**, *11* (6), 1053−1057.
(54) Humphrey, W.; Dalke, A.; Schulten, K. VMD: Visual Molecular Dynamics. *J. Mol. Graphics* **1996**, *14* (1), 33−38.
(55) Bhargava, B. L.; Balasubramanian, S. Dynamics in a Room-Temperature Ionic Liquid: A Computer Simulation Study of 1,3-Dimethylimidazolium Chloride. *J. Chem. Phys.* **2005**, *123* (14), 144505.
(56) Shi, R.; Wang, Y. Ion-Cage Interpretation for the Structural and Dynamic Changes of Ionic Liquids under an External Electric Field. *J. Phys. Chem. B* **2013**, *117* (17), 5102−5112.
(57) Casella, G.; Causin, V.; Rastrelli, F.; Saielli, G. Ionic Liquid Crystals Based on Viologen Dimers: Tuning the Mesomorphism by Varying the Conformational Freedom of the Ionic Layer. *Liq. Cryst.* **2016**, *43*, 1161−1173.

DOI: 10.1021/acs.jpcb.6b03379
J. Phys. Chem. B 2016, 120, 5678−5690